RESEARCH ARTICLE OPEN ACCESS

Plasma *N*-Glycan Profiling Enhances Diagnostic Precision in Multiple Sclerosis, AQP4-Ab NMOSD, and MOGAD

Tereza Kacerova,[1] Megan Sealey,[2] Luisa Saldana,[3] Wenzheng Xiong,[2] Mark R. Woodhall,[3] Patrick J. Waters,[3] Thomas Sénard,[4,5] Jack Cheeseman,[4] Paulina A. Urbanowicz,[4] Georgia Elgood-Hunt,[4] Daniel I.R. Spencer,[4] James S.O. McCullagh,[1] Maria Isabel Leite,[3] Gabriele C. DeLuca,[3] Jacqueline Palace,[3] Daniel C. Anthony,[2] Tianrong Yeo,[6,7,8] and Fay Probert[1]

Correspondence
Dr. Yeo
yeo.tianrong@singhealth.com.sg

Neurol Neuroimmunol Neuroinflamm 2025;12:e200502. doi:10.1212/NXI.0000000000200502

Abstract

Background and Objectives

Differentiating multiple sclerosis (MS) from antibody (Ab)-defined diseases, such as neuromyelitis optica spectrum disorders (NMOSDs), remains challenging, particularly as Ab levels decline. *N*-glycans play a key role in immunity, with changes in branching and fucosylation linked to T/B-cell function and MS onset while increased *N*-acetylglucosamine residues correlate with disease progression. Despite growing recognition of glycosylation in neuroinflammation, direct comparisons of the *N*-glycome between MS and Ab-defined diseases are lacking. This study aims to assess whether plasma *N*-glycome profiling can effectively differentiate these conditions and their subtypes.

Methods

This cohort study included 120 participants: 30 with relapsing-remitting MS (RRMS), 30 with secondary progressive MS (SPMS), 30 with myelin oligodendrocyte glycoprotein Ab–associated disease (MOGAD), and 30 with aquaporin-4 (AQP4)-Ab NMOSD, recruited from the John Radcliffe Hospital, Oxford University Hospitals National Health System (NHS) Trust. Plasma *N*-glycans were analyzed using ultra-high-performance (UHPLC) hydrophilic interaction liquid chromatography (HILIC) coupled with high-resolution mass spectrometry. Orthogonal partial least-squares discriminant analysis was applied to identify disease-specific glycomic patterns.

Results

Distinct *N*-glycome profiles were identified across diseases and phenotypes. Plasma *N*-glycans differentiated MS from Ab-defined diseases with 80.5% accuracy (±1.5%), MOGAD from AQP4-Ab NMOSD with 77.8% accuracy (±3.1%), and RRMS from SPMS with 75.2% accuracy (±3.6%). Key discriminatory features included increased monosialylation (S1; odds ratio [OR] = 2.57, $p < 0.0001$), trigalactosylation (G3; OR = 2.70, $p < 0.0001$), highly branched *N*-glycans (OR = 2.32, $p = 0.0002$), and antennary fucosylation (OR = 2.89, $p < 0.0001$), effectively distinguishing Ab-defined diseases from MS, independent of Ab serostatus at the time of sampling.

Discussion

These findings underscore the potential of plasma *N*-glycomics as a diagnostic tool for neuroinflammatory diseases. While further research is needed to clarify the mechanistic links between glycomic alterations and disease pathology, our results suggest that plasma *N*-glycan profiling could improve disease classification. Given its noninvasive and cost-effective nature, this approach holds promise as a complementary diagnostic tool for CNS demyelinating diseases in clinical practice.

MORE ONLINE

Supplementary Material

[1]Chemistry Research Laboratory, Department of Chemistry, University of Oxford, United Kingdom; [2]Department of Pharmacology, University of Oxford, United Kingdom; [3]Nuffield Department of Clinical Neurosciences, John Radcliffe Hospital, University of Oxford, United Kingdom; [4]Ludger Ltd, Culham Science Centre, Abingdon, United Kingdom; [5]Division of Endocrinology and Diabetes Prevention and Care, IRCCS Azienda Ospedaliero-Universitaria di Bologna, Italy; [6]Department of Neurology, National Neuroscience Institute, Singapore; [7]Duke-NUS Medical School, Singapore; and [8]Lee Kong Chian School of Medicine (Nanyang Technological University), Singapore.

The Article Processing Charge was funded by the authors.

Glossary

AF = antennary fucosylation; **APC** = antigen-presenting cell; **DMT** = disease-modifying therapy; **GJCF** = Guthy-Jackson Charitable Foundation; **HB** = high branching; **HILIC** = hydrophilic interaction liquid chromatography; **HRMS** = high-resolution mass spectrometry; **IgG** = immunoglobulin G; **LB** = low branching; **MOGAD** = myelin oligodendrocyte glycoprotein Ab–associated disease; **MS** = multiple sclerosis; **nFG** = nonfucosylated glycan; **NMOSD** = neuromyelitis optica spectrum disorder; **OPLS-DA** = orthogonal partial least-squares discriminant analysis; **OR** = odds ratio; **PPMS** = primary progressive MS; **RRMS** = relapsing-remitting MS; **SPMS** = secondary progressive MS; **VIP** = Variable Importance in Projection.

Introduction

The clinical and MRI overlap among multiple sclerosis (MS), aquaporin-4 (AQP4)–antibody (Ab) neuromyelitis optica spectrum disorder (NMOSD), and myelin oligodendrocyte glycoprotein Ab–associated disease (MOGAD) poses a diagnostic challenge, particularly at onset or when Ab titers have diminished.[1,2] While brain MRI can differentiate MS from AQP4-Ab NMOSD and MOGAD with high sensitivity and specificity,[1,3,4] many patients with AQP4-Ab NMOSD or MOGAD exhibit no detectable brain lesions. Ab testing remains the gold standard; however, Ab levels may fall below detection limits during remission or after immunotherapy,[1,4] highlighting the need for reliable biomarkers.[5] Accurate diagnosis is crucial because MS-specific therapies can trigger relapses in Ab-defined diseases,[6] while the availability of early high-efficacy MS treatments[7] and emerging monoclonal Ab therapies for AQP4-Ab NMOSD further underscores this need.[8-10] Distinguishing relapsing-remitting MS (RRMS) from secondary progressive MS (SPMS) relies on clinical assessment and disability indices such as the Expanded Disability Status Scale. However, early SPMS diagnosis lacks consensus on clinical thresholds and rely on long-term observation of irreversible disability progression. Emerging biofluid markers show promise but require further validation.[11-13]

NMR-based metabolomics of blood has been shown to accurately distinguish RRMS from AQP4-Ab NMOSD, MOGAD, and SPMS.[12-18] Glycoprotein A (GlycA), an NMR-specific marker of *N*-acetylglucosamine glycan residues linked to inflammation,[19] is elevated in SPMS,[12,13] suggesting that *N*-glycan structures may serve as markers of SPMS transition. Supporting this, MS patient plasma shows increased complex glycans, including galactose and sialic acid residues and antennary fucosylation (AF), compared with healthy controls.[20] Similarly, bisected and monogalactosylated (G1) glycans are more abundant in MS CSF.[21] However, *N*-glycome changes linked to MS progression remain unstudied. Likewise, despite known roles of *N*-glycans in T-cell and B-cell function and differences between Ab-mediated and cell-mediated diseases, direct comparisons of *N*-glycomes in MS vs Ab-defined diseases are lacking. *N*-glycans modulate immune responses through Fcγ receptor IIIa (FcγRIIIa), with glycan modifications influencing inflammation.[22] Reduced *N*-glycan branching has been shown to trigger autoimmunity and promote demyelination in murine models,[23] highlighting the potential of plasma *N*-glycome profiling to reveal mechanisms underlying disease onset and progression.

Using ultra-high-performance (UHPLC) hydrophilic interaction liquid chromatography (HILIC) coupled with high-resolution mass spectrometry (HRMS), we analyzed samples from a cohort of 30 patients with RRMS, 30 with SPMS, 30 with MOGAD, and 30 with AQP4-Ab NMOSD to identify *N*-glycan biomarkers for distinguishing MS from Ab-defined diseases, RRMS from SPMS, and MOGAD from AQP4-Ab NMOSD.

Methods

Study Participants and Procedures

Patients were recruited from the John Radcliffe Hospital, Oxford University Hospital Trust, United Kingdom. Patients with MS met the 2017 McDonald diagnostic criteria, while SPMS was diagnosed in individuals with a prior RRMS diagnosis and at least 1 year of disability progression without relapses.[24] AQP4-Ab NMOSD was diagnosed using the 2015 International Panel for NMO Diagnosis (IPND) criteria, with AQP4 Ab confirmed via a live cell-based assay.[25] MOGAD was diagnosed with MOG Ab positivity on a live cell-based assay in patients with at least 1 inflammatory demyelinating event compatible with MOGAD.[26] Blood samples were collected in lithium-heparin tubes (Becton Dickinson 367375), left at room temperature for 30 minutes, and then centrifuged at 1,300 g for 10 minutes, as previously described.[13] Plasma was aliquoted and stored at −80°C. A random subset of MS samples collected before April 2019 and Ab-defined disease samples collected before February 2018, with no prior freeze-thaw cycles, were selected for glycomics analysis.

Standard Protocol Approvals, Registrations, and Patient Consents

Patients were recruited as part of the Oxford METabolomics cohort, with consent obtained under the Oxford Radcliffe Biobank and ethical approval from the NRES Committee South Central–Oxford C (REC reference: 09/H0606/5 + 5).

HILIC-HRMS Analysis of *N*-Glycans

The HILIC-UHPLC-MS analysis was performed by Ludger Ltd., United Kingdom. A volume of 5 μL of either plasma (single aliquot), plasma standard (triplicate aliquot), or

immunoglobulin G (IgG) standard (triplicate aliquot) was added to each well of a skirted 96-well plate of 180-µL volume (4titide Ltd., United Kingdom). The plate was transferred to a liquid handling robot (Hamilton, Birmingham, United Kingdom) for semiautomatic processing. Recombinant PNGase F (P0709, New England Biolabs, United Kingdom) was used to release *N*-glycans from glycoproteins. Each sample was adjusted to a total volume of 9 µL by adding 4 µL of water, followed by the addition of 1 µL of denaturation buffer. The samples were vortexed and centrifuged before incubation at 37 °C for 16 hours. The resulting sample mixtures were dried using a vacuum centrifuge (Thermo Fisher Scientific, United Kingdom) for 2 hours at room temperature (RT). The glycans were converted to aldoses by addition of 20 µL of 1% formic acid solution (Sigma Aldrich, United Kingdom). The samples were vortexed and centrifuged before incubation for 45 minutes at room temperature. The samples were filtered through a LudgerClean 96-well protein-binding membrane plate (LC-PBM-96, Ludger Ltd., United Kingdom) with water (2 × 100 µL) to remove excess protein. The resulting 200-µL solutions were transferred to a nonskirted 96-well plate of 300-µL volume (4titude Ltd, United Kingdom) and dried down in a vacuum centrifuge for 9 hours at RT. The dried glycans were subjected to fluorescent labeling by reductive amination with 20 µL of procainamide labeling solution (LT-KPROC-96, Ludger Ltd., United Kingdom). The samples were vortexed and briefly centrifuged before incubation for 1 hour at 65 °C. The samples were mixed with 80 µL of acetonitrile (Romil Ltd., United Kingdom) before being transferred to a LudgerClean procainamide cleanup plate (LC-PROC-96, Ludger Ltd., United Kingdom) and washed with acetonitrile (3 × 100 µL) to remove excess labeling solution. The labeled glycans were recovered by washing with water (2 × 100 µL). For liquid chromatography-tandem mass spectrometry (LC-MS/MS) analysis, 100 µL of each sample was added to 300 µL of acetonitrile. System suitability standards (plasma, IgG, glucose homopolymer [GHP, Ludger Ltd., United Kingdom]) and blanks were prepared by adding 25 µL of each standard to 75 µL of acetonitrile. All samples were analyzed by HILIC-HRMS with fluorescence detection. A volume of 20 µL of each standard and sample was injected onto an ACQUITY UPLC BEH-Glycan column (1.7 µm, 2.1 mm × 150 mm; Waters, United Kingdom) at 40°C using a Thermo Fisher Scientific Vanquish UHPLC instrument with a fluorescence detector (λex = 310, λem = 370 nm), coupled to a Thermo Fisher Scientific Orbitrap Exploris 120 mass spectrometer. The chromatography conditions were as follows: solvent A 50 mM ammonium formate (pH 4.4) made from LudgerSep N-Buffer (Ludger Ltd., United Kingdom) and solvent B acetonitrile. Gradient conditions were as follows: 0–53.5 minutes, 76%–51% B, 0.4 mL/minute; 53.5–55.5 minutes, 51%–0% B, 0.4 mL/minute to 0.2 mL/minute; 55.5–57.5 minutes, 0% B at a flow rate of 0.2 mL/minute; 57.5–59.5 minutes, 0%–76% B, 0.2 mL/minute; 59.5–65.5 minutes, 76% B, 0.2 mL/minute; 65.5–66.5 minutes, 76% B, 0.2 mL/minute to 0.4 mL/minute; 66.5–70.0 minutes, 76% B, 0.4 mL/minute. The Exploris 120 settings were as follows: source vaporization temperature, 350°C; ion transfer tube temperature, 325°C; sheath gas, 50 arbitrary units (Arb); auxiliary gas, 10 Arb; sweep gas, 1 Arb; capillary voltage, 3500 V; and pos. ion mode. MS spectra were recorded in the mass range of 500 − 2,500 m/z, with a resolution of 1.5×10^4, using data-dependent acquisition mode and radiofrequency (RF) level of 70%.

HILIC-HRMS Data Processing

Fluorescence data were quantified using HappyTools (v0.1-beta1), based on peak area.[27] MS data were processed with LaCyTools (v1.1.0-alpha), using extracted ion chromatogram peak areas.[28] Signals meeting the criteria for mass accuracy (±10 ppm), isotopic pattern quality (IPQ <0.15), and signal-to-noise ratio (S/N > 27) were analyzed.

N-Glycan Nomenclature

The standard Oxford Glycan Notation was followed.[29] *N*-glycans comprise 2 linked *N*-acetylglucosamines (GlcNAc) and 3 mannose residues, which may be modified by fucose (F), core mannose (M), galactose (G), sialic acid (S), bisecting GlcNAc (B), and branching patterns (antenna–A), with numeric notation indicating residue counts.[29] Isomeric glycans were named by elution order (e.g., FA3G3S2 and FA3G3S2.1). *N*-galactosylation traits were calculated as the ratio of specific glycan peaks to the total glycan integral (e.g., G2/total*100).[20,30] A list of traits is provided in eTable 1.

Statistical Analysis

Curated LaCyTools-derived features were imported into R (v4.2.1), sum-normalized, standardized (mean-centered and scaled to unit variance), and analyzed using *in-house* R scripts and the *ropls* package.[31] To evaluate differences between groups, orthogonal partial least-squares discriminant analysis (OPLS-DA) was performed, initially using individual glycan signals and subsequently the derived glycan traits, with 10-fold cross-validation, 100 repetitions, and permutation testing.[13] Accuracy, sensitivity, and specificity were reported for independent test data not used in model training. For significant models (Kolmogorov-Smirnov test, $p < 0.05$), discriminatory variables were identified separately for glycans and glycan traits. The average Variable Importance in Projection (VIP) scores were assessed to quantify each variable's contribution to the model. Glycans and traits above the VIP inflection point were subjected to univariate analysis.

Odds ratios (OR) were calculated in R (v4.2.1) to assess the change in diagnosis probability per unit increase in glycan traits. Binary classification models evaluated trait-outcome relationships, and results were visualized as forest plots with 95% CIs. Remaining univariate analyses were conducted in GraphPad Prism 10. Continuous variables were compared using unpaired 2-sample *t* tests with false discovery rate (FDR) correction (Benjamini-Hochberg, $p < 0.05$), while categorical variables were analyzed using the χ^2 test. Data are presented as Tukey boxplots (with whiskers at 1.5 × interquartile range). For multiple group comparisons, one-way analysis of variance

(1W-ANOVA) with the Tukey post hoc test was applied, controlling for multiple comparisons ($p < 0.05$).

Data Availability

Anonymized data not published within this article will be made available by request to the corresponding author from any qualified investigator.

Results

Patient Characteristics

A total of 120 patients were included: 30 with RRMS, 30 with SPMS, 30 with MOGAD, and 30 with AQP4-Ab NMOSD. Demographic characteristics are summarized in Table 1.

Consistent with prevailing knowledge, women predominated across groups: RRMS, 60%; SPMS, 90%; MOGAD, 63%; and AQP4-Ab NMOSD, 90% ($p = 0.0016$).[32-34] Mean ages were as follows: AQP4-Ab NMOSD, 52 years; MOGAD, 38 years; RRMS, 45 years; and SPMS, 60 years ($p = 0.0002$), consistent with later onset in AQP4-Ab NMOSD and SPMS. Despite significant demographic differences (Table 1, eFigure 1, A–E), multivariate analysis showed that sex, age, disease duration, relapse timing, or medication did not enhance OPLS-DA model accuracy. Moreover, no strong correlations were found between discriminatory glycans and clinical variables ($R^2 < 0.20$, Spearman $\rho < 0.30$). All patients with AQP4-Ab NMOSD received immunosuppression, while 73% of patients with RRMS were on disease-modifying therapies (DMTs). MOGAD treatments included steroids (17%), immunosuppressants (17%), or both (20%). OPLS-DA score plots (eFigures 2–4) showed no clustering by medication, suggesting minimal impact of pharmacotherapy on glycomic profiles.

N-Glycomics Enables Accurate Discrimination Between MS and Ab-Defined Diseases

To assess the discriminatory potential of the human plasma *N*-glycome, we analyzed 120 HILIC-HRMS spectra (30 per condition—RRMS, SPMS, AQP4-Ab NMOSD, MOGAD). We initially focused on distinguishing participants diagnosed with MS (combining RRMS and SPMS) from those diagnosed with Ab-defined diseases (AQP4-Ab NMOSD and MOGAD). The ensemble of OPLS-DA models achieved a mean predictive accuracy of 80.5% ± 1.5% for MS vs Ab-defined diseases, significantly outperforming the randomly permuted ensemble (50.1% ± 6.5%, $p < 0.0001$) (Figure 1A), highlighting the discriminatory potential of the plasma *N*-glycome in discriminating between MS and Ab-defined diseases.

Plasma *N*-Glycomics as a Discriminatory Tool for RRMS, SPMS, MOGAD, and AQP4-Ab NMOSD

Given that the plasma *N*-glycome demonstrated robust discriminatory capacity in distinguishing MS from Ab-defined diseases, we assessed its ability to differentiate individual conditions. OPLS-DA models were built for pairwise comparisons (RRMS, SPMS, MOGAD, AQP4-Ab NMOSD), achieving consistently higher predictive accuracy than random class ensembles (Figure 1B). OPLS-DA successfully distinguished RRMS and SPMS from AQP4-Ab NMOSD, with accuracies of 92.7% ± 1.4% and 96.7% ± 0.8%, respectively. Significant differences were also observed between SPMS and MOGAD, achieving an accuracy of 75.8% ± 2.4%. The model distinguishing RRMS from MOGAD showed a separation accuracy of 57.3 ± 4.1%, while the model distinguishing RRMS from SPMS demonstrated an accuracy of 75.2% ± 3.6%. Furthermore, the plasma *N*-glycome effectively differentiated Ab-defined diseases based on Ab profiles, achieving an accuracy of 77.8% ± 3.1% for MOGAD vs AQP4-Ab NMOSD. All OPLS-DA models—with the exception of MOGAD vs RRMS—demonstrated high accuracy, sensitivity, and specificity, underscoring the diagnostic potential of glycan analysis. Notably, the separation among AQP4-Ab NMOSD, MOGAD, and MS was achieved independently of Ab serostatus at the time of sampling, with most seronegative AQP4-Ab NMOSD and MOGAD patients accurately classified (eFigure 5, A–E), supporting plasma *N*-glycome profiling as a robust, complementary diagnostic tool beyond traditional Ab markers. The most discriminatory 25 glycans for each model are summarized in eTable 2. Figure 2 displays chromatograms for each condition, highlighting the 3 glycan signals with the highest VIP score for each diagnostically relevant comparison.

The analysis of glycan signals with the highest VIP scores revealed that highly branched, complex glycans with multiple modifications—such as antennae structures, sialylation, and galactosylation—were consistently the most discriminatory across all comparisons. In the RRMS vs AQP4-Ab NMOSD model, the most distinctive glycans included A3G3S1.3 (1W-ANOVA $p < 0.0001$) (eFigure 6A), which was markedly elevated in AQP4-Ab NMOSD, as well as FA2BG2S1.1 (1W-ANOVA $p < 0.0001$) (eFigure 6B) and FA3G3S3.3 (1W-ANOVA $p = 0.001$) (eFigure 6C), both of which were significantly reduced in AQP4-Ab NMOSD compared with the other groups. In the RRMS vs MOGAD model, the primary discriminatory features were unresolved chromatographic peaks (eTable 2). Among the assigned glycans, the most distinctive were A3G3S1.4 (1W-ANOVA $p = 0.001$) (eFigure 6D), A2G2S2.5 (1W-ANOVA $p = 0.008$) (eFigure 6E), and FA3G3S2.5 (1W-ANOVA $p < 0.0001$) (eFigure 6F). In the RRMS vs SPMS model, glycan abundance changes were less pronounced, with A4G4S1 (1W-ANOVA $p = 0.007$) (eFigure 6 G), A3G3S2 (1W-ANOVA $p = 0.003$) (eFigure 6H), and FA3G3S1.1 (1W-ANOVA $p = 0.002$) (eFigure 6I) being the most discriminatory. The AQP4-Ab NMOSD vs MOGAD model was primarily driven by highly modified, fucosylated glycans, such as FA3G3S3.5 (1W-ANOVA $p < 0.0001$) (eFigure 6J), FA3G3S3.2 (1W-ANOVA $p < 0.0001$) (eFigure 6K), and FA2BG2S1.2 (1W-ANOVA $p < 0.0001$) (eFigure 6L). Notably, 1W-ANOVA (particularly eFigure. 6, J and K) revealed significant differences in abundance for AQP4-Ab NMOSD compared with the other 3 groups. This suggests that AQP4-Ab NMOSD is the primary driver of separation in the MS vs Ab-defined disease model (Figure 1A), a conclusion

Table 1 Demographic Characteristics of Individuals With RRMS, SPMS, MOGAD, and AQP4-Ab NMOSD

	RRMS n = 30	SPMS n = 30	MOGAD n = 30	AQP4-Ab NMOSD n = 30	*p* Value
Female, n (%)	18 (60)	27 (90)*	19 (63)	27 (90)*, †	0.0016
Age (y)[a]	45.18 ± 10.12	59.86 ± 9.90***, †††	37.52 ± 11.93	51.67 ± 17.05†††	0.0002
BMI (kg/m^2)[a]	27.95 ± 7.64	25.81 ± 7.07	27.72 ± 5.55	28.89 ± 8.05	0.429
EDSS score[a]	3.38 ± 1.75††	6.67 ± 1.04***, †††	1.92 ± 1.34	3.78 ± 2.22†††	<0.0001
Disease duration (y)[a]	13.04 ± 10.03	31.80 ± 10.64***, †††	8.52 ± 10.53	8.53 ± 6.24	<0.0001
Time since last relapse (y)[a]	3.69 ± 3.18	11.67 ± 6.67***, †††	2.12 ± 2.41	3.13 ± 2.31	<0.0001
Ab positivity status[a] at the time of sampling	NA	NA	22/30[b]	24/30[b]	NA
MS disease-modifying therapies (DMTs) n (%)	22 (73)	2 (7)	0 (0)	0 (0)	NA
	Interferon beta-1a (4)	Interferon beta-1a (1)	—	—	
	Glatiramer acetate (10)	Peginterferon beta 1a (1)	—	—	
	Alemtuzumab (2)	—	—	—	
	Dimethyl fumarate (3)	—	—	—	
	Natalizumab (2)	—	—	—	
	Fingolimod (1)	—	—	—	
Corticosteroids, n (%)	1 (3)	1 (3)	11 (37)[c]	0 (0)	NA
	Prednisolone (1)	Betamethasone (1)	Prednisolone (11)	—	
Immunosuppression n (%)	0 (0)	0 ()	11 (37)	30 (100)	NA
	—	—	Azathioprine (6)	Mycophenolate mofetil (9)	
	—	—	Methotrexate (2)	Azathioprine (10)	
	—	—	Tocilizumab (1)	Methotrexate (5)	
	—	—	Mycophenolate mofetil (1)	Rituximab (3)	
	—	—	IVIG (1)	Mycophenolate mofetil + Rituximab (3)	

Abbreviations: BMI = body mass index; EDSS = Expanded Disability Status Scale; IVIG = intravenous immunoglobulin; MOGAD = myelin oligodendrocyte glycoprotein Ab–associated disease; NMOSD = neuromyelitis optica spectrum disorder; RRMS = relapsing-remitting MS; SPMS = secondary progressive MS. χ^2 and one-way ANOVA *p* values are reported for categorical and continuous variables, respectively. Tukey post hoc *p* values <0.05, 0.01, and 0.001 relative to RRMS are represented by *, **, and ***, while significant differences relative to MOGAD are represented by †, ††, and †††. A summary of all post hoc results are displayed in eFigure 1, A–E. Age, BMI, EDSS score, and time since last relapse are given as mean ± SD.

[a] The indicated values are recorded at the sampling point.

[b] Seronegative MOGAD patients had previously tested positive for MOG Ab but were seronegative at the time of sampling, consistent with the fluctuating serostatus observed in MOGAD. Patients with AQP4-Ab NMOSD who were previously positive for AQP4 Ab but with Ab titers ≤1:20 at time of sampling were classified as seronegative.

[c] Of the 11 patients with MOGAD receiving corticosteroid therapy, 6 also received immunosuppressive treatment (azathioprine: 4, methotrexate: 1, IVIG: 1).

supported by the high accuracy of the AQP4-Ab NMOSD vs RRMS and AQP4-Ab NMOSD vs SPMS models (Figure 1B).

N-Glycan Traits Differentiate MS From Ab-Defined Diseases, Highlighting Branching and Sialylation Patterns

To further understand the observed changes in the glycomic profiles, OPLS-DA was applied to *N*-glycosylation-derived traits (eTable 1). While the accuracy of these models decreased by an average of 5%–10% compared with those trained on all glycan signatures, except for the RRMS vs MOGAD model where the accuracy of the glycan trait–based model increased, this decline was likely due to the reduced number of variables and the loss of diagnostically relevant information when consolidating individual signals (eTable 3). Nevertheless, all models

Figure 1 *N*-Glycome Discriminates MS, Ab-Defined Diseases, and Their Phenotypes

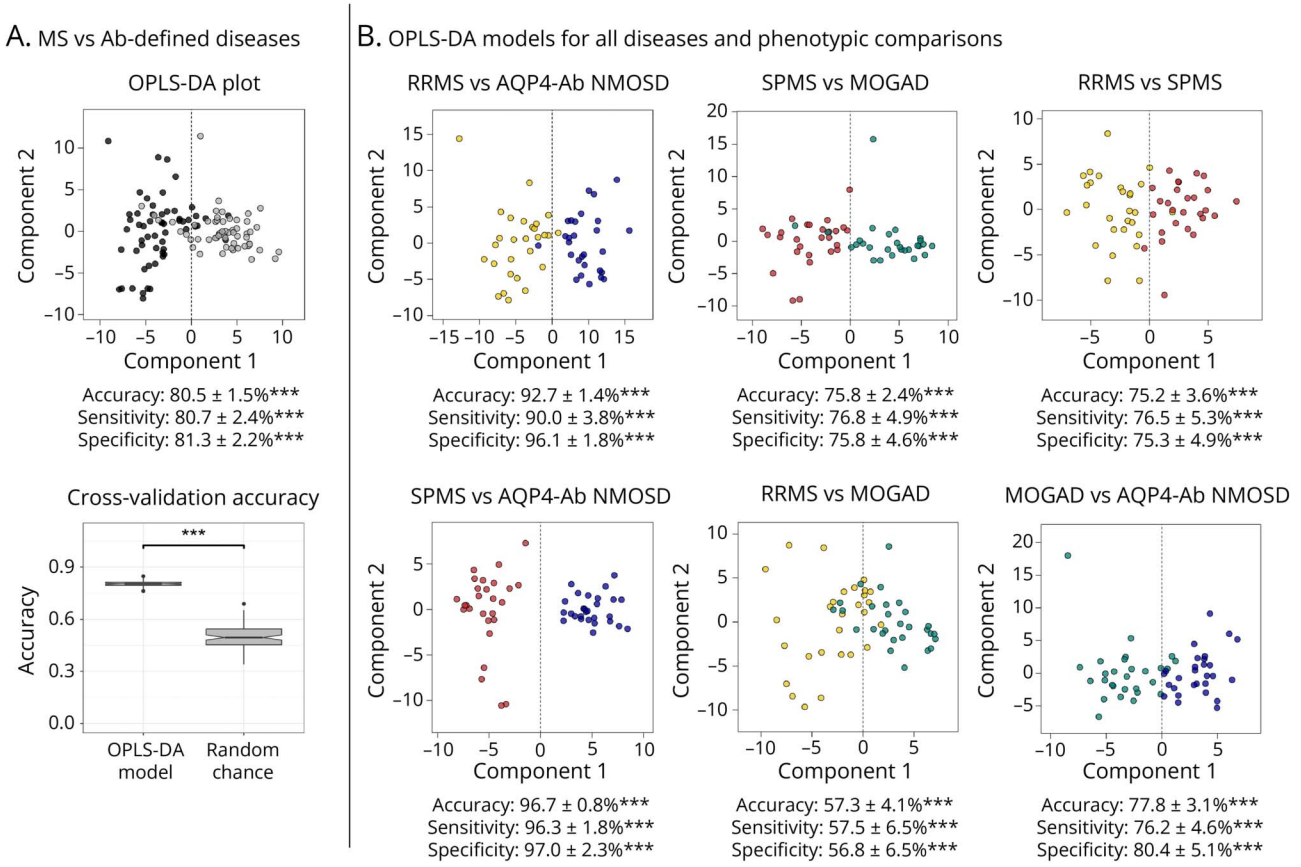

(A) OPLS-DA score plot illustrating distinct separation of MS (RRMS and SPMS combined, n = 60, black) and Ab-defined disease (MOGAD and AQP4-Ab NMOSD combined, n = 60, gray) plasma *N*-glycomes (model accuracy: 80.5% ± 1.5%; specificity: 81.3% ± 2.2%; sensitivity: 80.7% ± 2.4%). The accuracy of the ensemble comprising 1000 MS vs Ab-defined disease models, assessed through an independent test set classification, significantly surpassed that of the 1,000 randomly permuted models. Significance was determined by the Kolmogorov-Smirnov test (***$p < 0.0001$). (B) OPLS-DA score plots demonstrating patient differentiation based on plasma glycomic profiles for RRMS (yellow), SPMS (red), MOGAD (teal), and AQP4-Ab NMOSD (blue) across all permutations. Each model includes accuracy, sensitivity, and specificity parameters derived from cross-validation. Significance relative to a random class ensemble was determined by the Kolmogorov-Smirnov test (***$p < 0.0001$). MOGAD = myelin oligodendrocyte glycoprotein Ab–associated disease; OPLS-DA = orthogonal partial least-squares discriminant analysis; RRMS = relapsing-remitting MS; SPMS = secondary progressive MS.

outperformed the random class ensemble, allowing for a detailed examination of the discriminatory traits identified through the VIP scores (eTables 4–8).

OPLS-DA successfully distinguished MS from Ab-defined diseases based solely on *N*-glycan traits, achieving an accuracy of 71.5% ± 2.5%, sensitivity of 71.7% ± 3.3%, and specificity of 72.4% ± 3.4%. The most discriminatory traits were primarily associated with variations in galactosylation and fucosylation (Figure 3, A and B) (eTable 4): monosialylation excluding hybrids (S1-H, $p < 0.0001$; OR = 2.63), trigalactosylation in nonfucosylated glycans (nFG3, $p < 0.0001$; OR = 3.03), monosialylation (S1, $p < 0.0001$; OR = 2.57), monosialylation in nonfucosylated glycans (nFS1, $p < 0.0001$; OR = 2.89), trigalactosylation (G3, $p < 0.0001$; OR = 2.70), and AF ($p < 0.0001$; OR = 2.89) were decreased in MS compared with Ab-defined diseases, while trisialylation (S3, $p = 0.0004$; OR = 0.27) and trisialylation of fucosylated glycans (FS3, $p = 0.0005$; OR = 0.296) were elevated in MS. Notably, the complexity of glycan branching emerged as one of the key discriminatory features, with MS characterized by higher levels of low branching (LB) glycans ($p = 0.0001$; OR = 0.41) and LB excluding hybrids (LB-H, $p = 0.0001$; OR = 0.39), and lower levels of high branching (HB) glycans ($p = 0.0002$; OR = 2.32), compared with Ab-defined diseases (Figure 3, A and B).

We then focused on identifying glycan traits that differentiate the individual conditions. Because SPMS is a distinct progressive stage, the key comparisons centered on differentiating RRMS from MOGAD and AQP4-Ab NMOSD, which is particularly relevant for early disease classification. The OPLS-DA model, based exclusively on glycan traits, demonstrated significant differentiation between RRMS and AQP4-Ab NMOSD, achieving an accuracy of 86.3% ± 2.2%. Notably, most of the discriminatory traits (Figure 4A) (eTable 5) overlapped with those identified in the MS vs Ab-defined disease model (Figure 3B). AF ($p = 0.0004$; OR = 3.63) (Figure 5A) and G3 ($p = 0.0004$; OR = 3.82) (Figure 5A) were significantly decreased in RRMS compared with AQP4-

Figure 2 Representative HILIC-HRMS Fluorescence Profiles of Individuals With RRMS, SPMS, MOGAD, and AQP4-Ab NMOSD

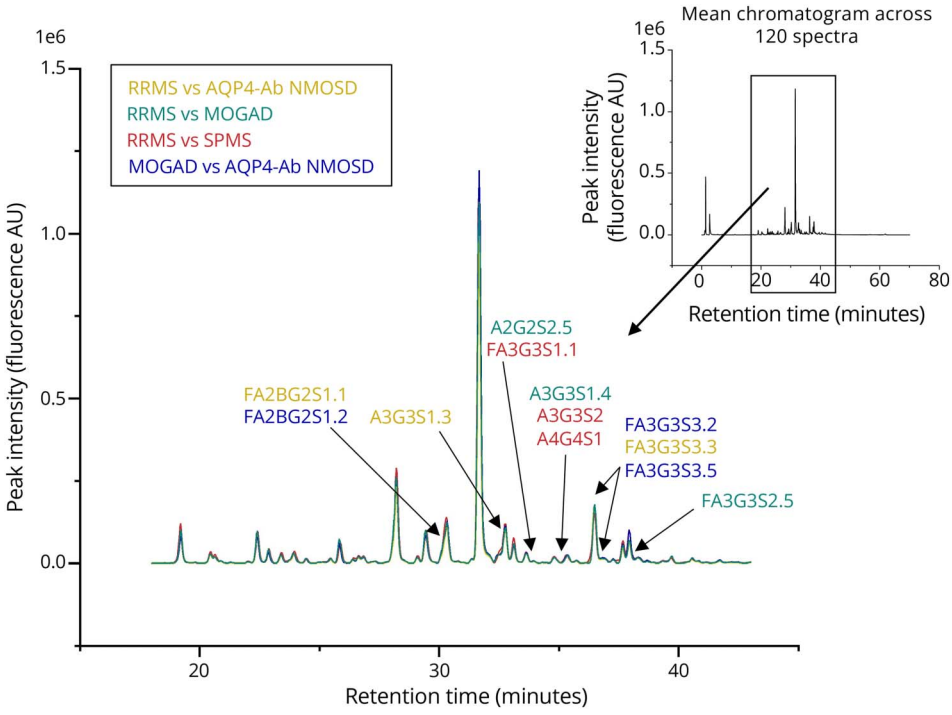

The complete chromatogram is displayed in the top right corner, with a magnified view of the elution region (18–43 minutes), where most glycan species are identified. Each chromatogram represents the average of 30 samples per condition: RRMS (yellow); SPMS (red); MOGAD (teal); AQP4-Ab NMOSD (blue). Three glycan signals (note: some co-elute within a multiple glycan peak) with the highest VIP score are highlighted for each diagnostically relevant comparison: RRMS vs AQP4-Ab NMOSD (yellow); MOGAD vs RRMS (teal); SPMS vs RRMS (red); AQP4-Ab NMOSD vs MOGAD (blue). The inset shows the overlay of the averaged chromatogram across all 120 spectra. MOGAD = myelin oligodendrocyte glycoprotein Ab–associated disease; NMOSD = neuromyelitis optica spectrum disorder; RRMS = relapsing-remitting MS; SPMS = secondary progressive MS.

Ab NMOSD (eFigure 7). Furthermore, the inverse relationship between HB and LB glycans was conserved, with HB decreased (p = 0.0010; OR = 3.16) and LB increased (p = 0.0010; OR = 0.30) in RRMS. S3, previously identified as a discriminatory trait between MS and Ab-defined diseases, was elevated in RRMS, although the OR was relatively modest (p = 0.0270; OR = 0.39). Similarly, although S1, identified as discriminatory in the MS vs Ab-defined disease model, did not feature among the top VIP scores in the RRMS and AQP4-Ab NMOSD model, it exhibited the same trend (p = 0.0173; OR = 2.40). It is important to note that assessing S1 for nonhybrid structures only (S1-H) significantly increased the OR (p = 0.0101; OR = 2.67). Conversely, digalactosylation in fucosylated glycans (FG2), which was not a discriminatory trait in the MS vs Ab-defined disease model, was highly discriminatory in this comparison (p = 0.0004; OR = 0.24) (Figure 5A). Finally, the ratio of fucosylated to nonfucosylated agalactosylated glycans (FG0/G0) was significantly increased in RRMS, despite being associated with high variability (p < 0.0001; OR = 0.015) (eFigure 7).

The OPLS-DA model for RRMS vs MOGAD was the only comparison where accuracy increased when using glycan traits alone, achieving an accuracy of 67.6% ± 2.9%. The identified discriminatory glycan traits (Figure 4B) (eTable 6) were consistent with the findings from the RRMS vs AQP4-Ab NMOSD model and closely mirrored the results from the general MS vs Ab-defined disease model (Figure 3B). The most discriminatory glycan traits were identified as S1 (p = 0.0503; OR = 2.42) (Figure 5B), S1-H (p = 0.0331; OR = 2.24) (Figure 5B), AF (p = 0.0720; OR = 2.10), and nFG3 (p = 0.0720; OR = 2.31), all of which were decreased in RRMS compared with MOGAD. Conversely, S3 (p = 0.0331; OR = 0.20) (Figure 5B), FS3 (p = 0.0704; OR = 0.19), tetragalactosylation (G4, p = 0.1374; OR = 0.49), and the ratio of fucosylated to nonfucosylated trigalactosylated glycans (FG3/G3, p = 0.0704; OR = 0.46) were all significantly elevated in RRMS (Figure 4B).

We further aimed to identify key glycan traits associated with MS, with a specific focus on distinguishing between RRMS and SPMS profiles (Figure 4C). Compared with the Ab-defined disease group, patients with MS—particularly those with SPMS—were characterized by elevated levels of high mannose-content glycans (M, p = 0.0473; OR = 0.38) (Figure 5C), with higher concentrations observed in the SPMS group. Although the RRMS vs SPMS model showed relatively high discriminatory capacity using all glycan signals (accuracy 75.8% ± 2.4%) (Figure 1B), the accuracy decreased to 62.2% ± 3.8% when only glycan traits were considered. This decline in accuracy corresponded to a lower number of significantly altered glycan traits (Figure 4C) (eTable 7). Among the glycan traits highlighted by the VIP scores, significant changes were observed in the ratio between monosialylated and disialylated fucosylated glycans, which was elevated in the SPMS group (FS1/FS2, p = 0.0004; OR = 0.24) (Figure 5C). Other discriminatory traits included FG0/G0 (p = 0.0473; OR = 2.19) (Figure 5C) and disialylation in

Figure 3 Key Glycan Traits Driving Separation Between MS and Ab-Defined Diseases Based on OPLS-DA VIP Scores and Statistical Significance

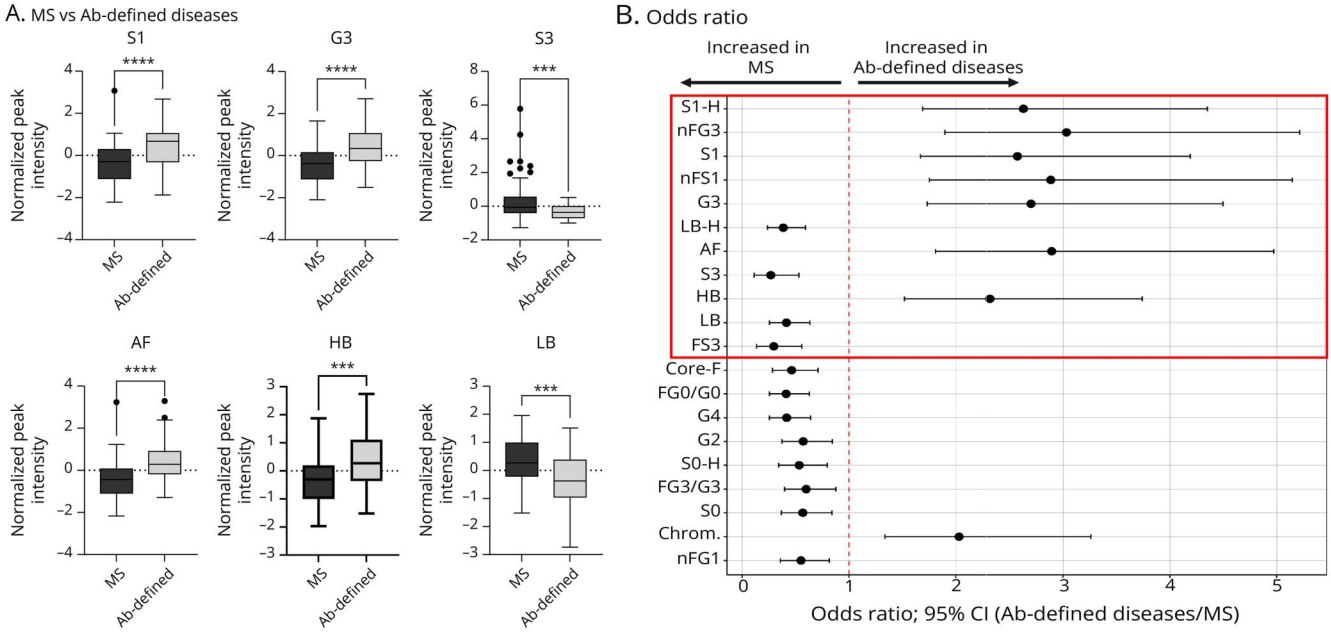

(A) Results from the unpaired 2-sample *t* test (FDR-corrected) are provided with significance levels (***$p < 0.001$; ****$p < 0.0001$). S1 ($p < 0.0001$); G3 ($p < 0.0001$); S3 ($p = 0.0004$); AF ($p < 0.0001$); HB ($p = 0.0002$); LB ($p = 0.0001$). (B) Calculated OR (given for Ab-defined diseases/MS) for each glycan trait along with 95% CI. Traits with OR greater than 1 were increased in Ab-defined diseases, while traits with OR less than 1 were increased in MS. The red box highlights traits with the highest VIP scores, determined by the inflection point cutoff and ranked accordingly. AF = antennary fucosylation; G2–G4 = digalactosylation to tetragalactosylation; H = hybrids; HB = high branching; LB = low branching; nFG1 = monogalactosylation in nonfucosylated glycans; nFG3 = trigalactosylation in nonfucosylated glycans; nFS1 = monosialylation of nonfucosylated glycans; OR = odds ratio; S0 = neutral glycans; S1 = monosialylation; S3 = trisialylation; chrom. = sum of unresolved chromatographic peaks.

fucosylated glycans (FS2, $p = 0.1067$; OR = 1.95), which were elevated in the RRMS group, while disialylation in nonfucosylated glycans (nFS2, $p = 0.0473$; OR = 0.44), G4 ($p = 0.1413$; OR = 0.54), and monogalactosylation in fucosylated glycans (FG1, $p = 0.7231$; OR = 0.66) were increased in the SPMS group.

For discrimination between MOGAD and AQP4-Ab NMOSD, model accuracy decreased to 74.5% ± 3.0% when only traits-derived information was used. Examination of glycan traits with the highest VIP scores (Figure 4D) (eTable 8) revealed that disialylation was among the most discriminatory features, with both S2 ($p = 0.0188$; OR = 0.35) (Figure 5D) and nFS2 ($p = 0.0236$; OR = 0.43) significantly increased in AQP4-Ab NMOSD compared with MOGAD. Other prominent glycan traits included FG0/G0 ($p < 0.0001$; OR = 24.57) (eFigure 8) and sialylation of fucosylated galactosylated glycans (FGS/(FG + FGS), $p = 0.0188$; OR = 2.30) that were elevated in individuals with MOGAD. A similar trend was observed for FG2 ($p = 0.0222$; OR = 2.41) while an inverse trend was noted for the related trigalactosylation in fucosylated glycans (FG3, $p = 0.0236$; OR = 0.44). In addition, monogalactosylation in nonfucosylated glycans (nFG1, $p = 0.0188$; OR = 2.43) and the level of bisecting GlcNAc in nonfucosylated glycans (nFB, $p = 0.0188$; OR = 2.21) (Figure 5D) were significantly decreased in AQP4-Ab NMOSD. In contrast to models focusing on MS vs Ab-defined diseases, the model centered solely on Ab-defined diseases identified mannose-containing (M-content) glycans and hybrids (H) as highly discriminatory, both of which were elevated in MOGAD (M-content: $p = 0.0188$; OR = 2.30; H: $p = 0.0276$; OR = 1.94, Figure 5D)).

These results indicate that specific glycan species are more abundantly expressed on plasma glycoproteins in patients with MS compared with those with Ab-defined diseases. Figure 6 comprehensively illustrates the overlap of individual glycan traits and summarizes the significantly altered profiles across conditions, as determined by VIP scores from the multivariate models.

Discussion

Current diagnostic techniques for MS, MOGAD, and AQP4-Ab NMOSD rely on clinical evaluation, Ab detection, and imaging.[1,2,35-37] Although effective, these approaches may be limited by accuracy, cost, and availability. Our previous studies across multiple independent cohorts demonstrated that NMR-based blood metabolomics can reliably distinguish MS from Ab-defined diseases and differentiate RRMS from SPMS, with significant differences also observed in *N*-glycan

Figure 4 Odds Ratios for Key Glycan Traits Distinguishing MS and Ab-Defined Disease Phenotypes

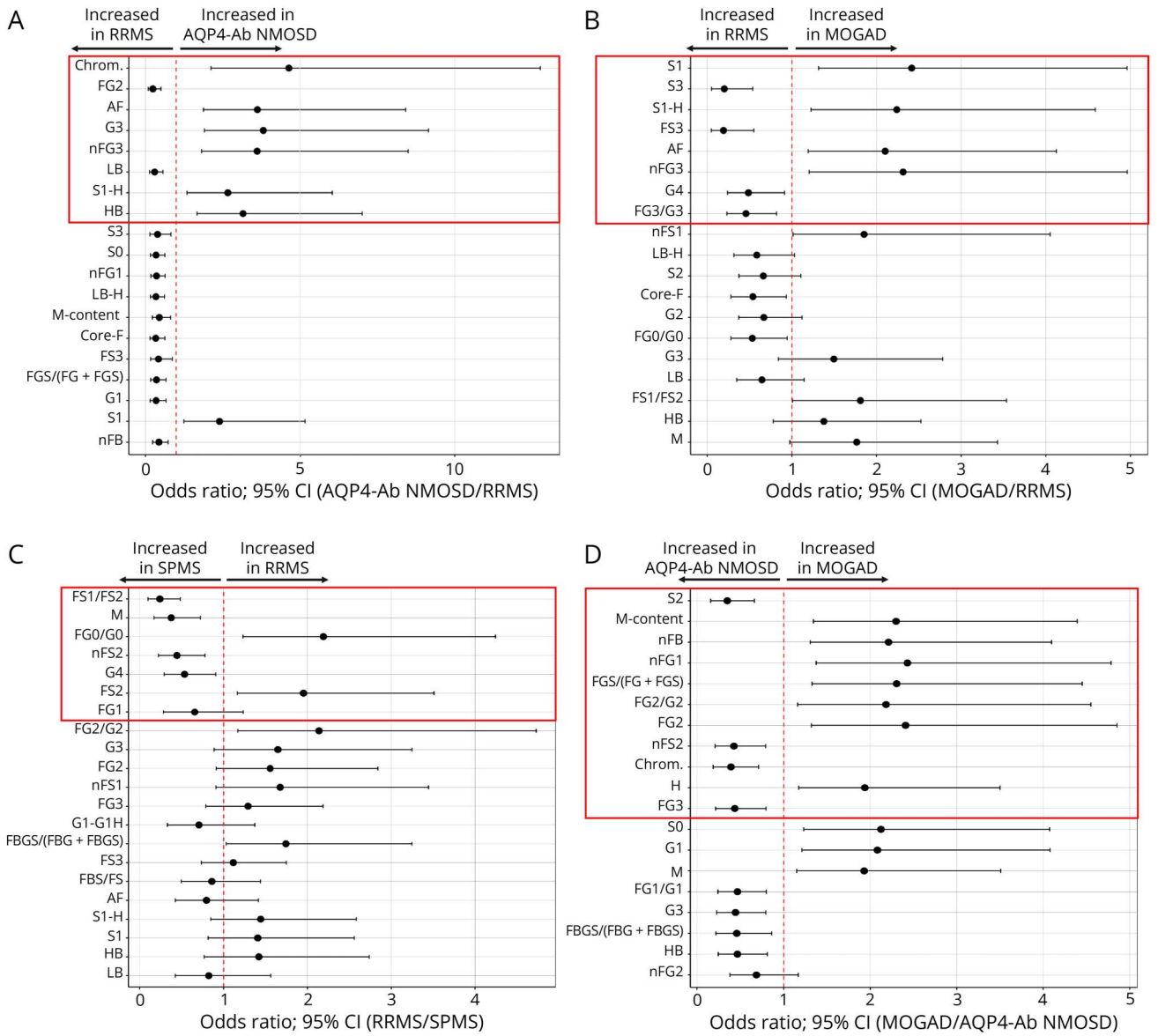

OR for the individual traits along with 95% CI for (A) AQP4-Ab NMOSD/RRMS, (B) MOGAD/RRMS, (C) RRMS/SPMS, and (D) MOGAD/AQP4-Ab NMOSD. The red box highlights the traits with the highest VIP scores (based on the inflection point cutoff; the individual traits are ordered based on the corresponding VIP score). Note: In panels (A) and (C), the FG0/G0 trait was excluded because of high variability (the forest plots in eFigures 7 and 8). AF = antennary fucosylation; FG0/G0 = ratio of fucosylated to nonfucosylated glycans; FG1–FG2 = monogalactosylation and digalactosylation in fucosylated glycans; FG2/G2 = ratio of fucosylated to nonfucosylated digalactosylated glycans; FGS/FG + FGS = sialylation of fucosylated galactosylated structures; FS1/FS2 = ratio of fucosylated monosialylated to disialylated glycans; FS2–FS3 = disialylation to trisialylation of fucosylated glycans; G1–G4 = monogalactosylation to tetragalactosylation; H = hybrids; HB = high branching; LB = low branching; M = high mannose; M-content = mannose-containing; nFB = bisecting nonfucosylated glycans; nFG1–nFG3 = monogalactosylation to trigalactosylation in nonfucosylated glycans; nFS2 = disialylation of nonfucosylated glycans; S0–S3 = neutral to trisialylated glycans; chrom. = sum of unresolved chromatographic peaks.

side-chain resonances between RRMS and SPMS.[13,16,18] Given the established link between altered glycosylation and neuroinflammation,[38,39] we investigated the diagnostic potential of *N*-glycans in MS and Ab-defined diseases.

Plasma *N*-glycome profiling effectively differentiates MS from Ab-defined diseases with 81% accuracy. Key discriminatory features include sialylation (S1, S1-H, S3), galactosylation, and AF, with the most pronounced alterations observed in AQP4-Ab NMOSD. Glycan branching also emerged as a distinguishing factor, with HB glycans significantly elevated in Ab-defined diseases, particularly in RRMS compared with AQP4-Ab NMOSD. However, limited clinical research on glycosylation in MS[17,20,21,40] and even scarcer data on MOGAD and AQP4-Ab NMOSD[41] present challenges for direct comparisons. Existing studies often involve mixed cohorts, complicating subtype-specific analyses. A previous study reported increased HB glycans in patients with MS compared with healthy controls but found no significant differences across MS stages,[20] partially aligning with our

Figure 5 Top Discriminatory *N*-Glycan Traits From Each Diagnostic Model Based on 1W-ANOVA With FDR Correction and the Tukey Post hoc Test

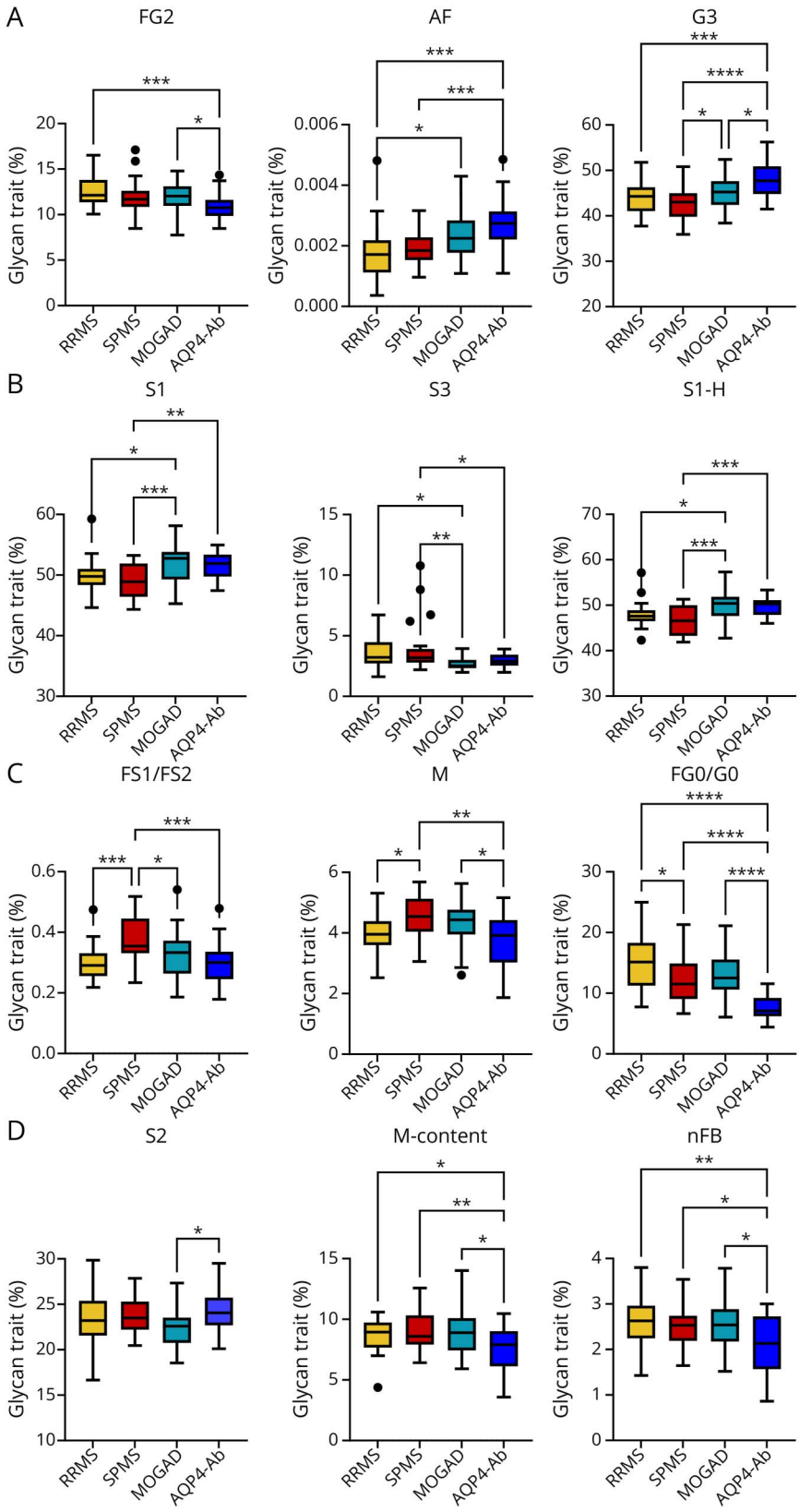

Results detailed in eTable 9. (A) AQP4-Ab NMOSD vs RRMS: FG2 (p = 0.002); AF (p < 0.0001); G3 (p < 0.0001). (B) MOGAD vs RRMS: S1 (p = 0.0003); S3 (p = 0.003); S1-H (p = 0.0003). (C) RRMS vs SPMS: FS1/FS2 (p < 0.0001); M glycans (p = 0.002); FG0/G0 (p < 0.0001). (D) AQP4-Ab NMOSD vs MOGAD: S2 (p = 0.02); M-content (p = 0.003); nFB (p = 0.003). AF = antennary fucosylation; FG0/G0 = ratio of fucosylated to nonfucosylated agalactosylated glycans; FG2 = digalactosylation in fucosylated glycans; FS1/FS2 = ratio of fucosylated monosialylated to disialylated glycans; G3 = trigalactosylation; M = high mannose; M-content = mannose-containing; nFB = incidence of bisecting nonfucosylated glycans; S1 = monosialylation; S1-H = monosialylation excluding hybrids; S2 = disialylation, and S3 = trisialylation.

findings. Although glycan branching patterns effectively distinguished MS from Ab-defined diseases, with elevated HB glycans in the latter, no significant differences were detected across MS subtypes. The elevated levels of HB glycans in Ab-defined diseases may appear counterintuitive, given rodent studies showing that *N*-glycan branching can reduce B cell–mediated inflammation and demyelination.[23] Similarly, *N*-glycan branching on antigen-presenting cells (APCs) has been shown to modulate their function, leading to reduced B-cell APC-induced proinflammatory responses and cytokine release.[23] Furthermore, a recent study reported that oral GlcNAc supplementation in patients with MS led to increased *N*-glycan branching, along with a reduction in serum levels of proinflammatory cytokines and neurofilament light chain.[22] The discrepancies between experimental and clinical findings highlight the complexity of these conditions and the challenges of comparing diverse cohorts and glycosylation analyses. Our findings reveal subtype-specific patterns, but validation in larger, standardized cohorts is needed to enhance clinical applicability.

G3 structures (independent of fucosylation) were significantly increased in Ab-defined diseases, particularly in AQP4-Ab NMOSD, whereas G1, G2, and G4 showed the opposite trend. Monogalactosylated, digalactosylated, and trigalactosylated glycans have been shown to reduce inflammation via natural killer cell FcγRIIIa and complement component C5a inhibition,[42] yet some may also act as inflammatory markers, although their roles remain unclear.[42]

Sialylation patterns, including S1 and S3, demonstrated discriminatory potential, with S1 and S1-H elevated in MOGAD compared with RRMS, while S3 traits were decreased in MOGAD, independent of fucosylation. Notably, S2 distinguished AQP4-Ab NMOSD from MOGAD, with lower levels in MOGAD. Sialylation plays a key role in modulating inflammation, as hyposialylated IgG is associated with chronic inflammation, whereas highly sialylated IgG exerts anti-inflammatory effects via FcγRIIIa.[42,43]

Fucosylation, in combination with galactosylation and sialylation, emerged as one of the most discriminatory glycan traits across multiple models. One study reported increased core fucosylation in patients with MS vs healthy controls,[20] while we observed significant fucosylation changes, with reduced AF in MS, distinguishing it from Ab-defined diseases. The FG0/G0 ratio separated RRMS from SPMS, whereas FG2/G2 distinguished MOGAD from AQP4-Ab NMOSD. Fucosylation is a key post-translational modification linked to inflammation.[42] It has been demonstrated that increased core fucosylation of IgG1-Fc inhibits FcγRIIIa interaction, reducing Ab-dependent cytotoxicity and promoting anti-inflammatory effects.[44] Conversely, another study found that reduced fucosylation in M1 macrophages facilitates inflammation resolution in rheumatoid arthritis.[45] Although fucosylation-derived traits are emerging as biomarkers in CNS diseases, their precise role warrants further investigation.

While elevated mannose levels have been reported in the *N*-glycome of patients with MS compared with healthy controls,[20] mannose was not among the most discriminatory features distinguishing MS from Ab-defined diseases. However, M structures strongly differentiated RRMS from SPMS, with higher levels in SPMS. In addition, total mannose, including

Figure 6 Overview of Discriminatory *N*-Glycan Traits Across MS and Ab-Defined Disease Phenotypes

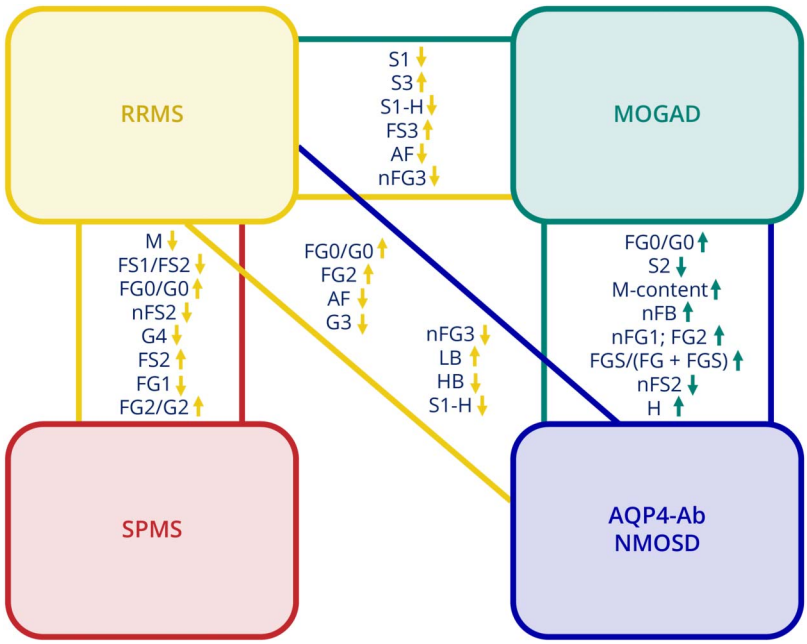

Arrows indicate increases (↑) or decreases (↓) in specific glycan traits within the patient group represented by the corresponding color: RRMS (yellow); SPMS (red); MOGAD (teal); AQP4-Ab NMOSD (blue). Lines connecting groups illustrate how glycan traits change when comparing groups, with the arrow's direction indicating the change with respect to the starting group (e.g., the yellow arrow on the yellow-to-red line shows glycan trait changes in RRMS, relative to SPMS). Glycan traits distinguishing SPMS from Ab-defined diseases (MOGAD and AQP4-Ab NMOSD) are omitted for clarity because these are less relevant for clinical diagnostic purposes. AF = antennary fucosylation; FG0/G0 = ratio of fucosylated to non-fucosylated glycans; FG1–FG2 = monogalactosylation and digalactosylation in fucosylated glycans; FG2/G2 = ratio of fucosylated to non-fucosylated digalactosylated glycans; FGS/FG + FGS = sialylation of fucosylated galactosylated structures; FS1/FS2 = ratio of fucosylated monosialylated to disialylated glycans; FS2–FS3 = disialylation to trisialylation of fucosylated glycans; G3–G4 = trigalactosylation to tetragalactosylation; H = hybrids; HB = high branching; LB = low branching; M = high mannose glycans; M-content = mannose-containing; nFB = bisecting nonfucosylated glycans; nFG1–nFG3 = monogalactosylation to trigalactosylation in non-fucosylated glycans; nFS2 = disialylation of non-fucosylated glycans; S1–S3 = monosialylation to trisialylation.

M-based hybrids, effectively distinguished MOGAD from AQP4-Ab NMOSD, with lower levels observed in the latter. Mannose-rich glycans activate complement via mannose-binding lectin,[46] and complement overactivation has been linked to microglia-driven pathology in progressive MS.[47] These associations suggest that M glycans may play a role in distinct inflammatory pathways in Ab-defined diseases.

The limited consideration of disease phenotypes in previous studies has left gaps in blood glycome data for MS and Ab-defined diseases, hindering direct comparisons. Our study focused on patients in a stable disease state and does not capture glycosylation dynamics during active relapse. A study showed that gut-derived IgA^+ B and plasma cells are recruited to the CNS during active MS, suggesting transient glycan reactivities linked to acute neuroinflammation.[48] These relapse-associated shifts may involve glycosylation changes, warranting future investigation. We did not include healthy controls because the aim was to determine whether plasma *N*-glycome profiling can differentiate CNS demyelinating diseases—rather than distinguish pathologic phenotypes from physiologic baseline. Patients with primary progressive MS (PPMS) were also not included because this phenotype is typically distinguishable clinically. Given the neuropathologic overlap between PPMS and SPMS,[49] some glycomic features may be shared, although further validation is needed. While no significant effects of DMTs were observed, small sample sizes may have obscured subtle influences. Nonetheless, this study uniquely explores the diagnostic potential of blood glycomics in well-defined CNS demyelinating diseases and provides new insights into neuroinflammatory mechanisms. Future work should validate findings in larger cohorts and incorporate CSF profiling to assess correlations with intrathecal immune activity.

In conclusion, plasma *N*-glycomics can distinguish MS and Ab-defined disease phenotypes, revealing immune signatures that may inform future targeted therapies.

Acknowledgment

The authors thank all patients who participated in this study.

Author Contributions

T. Kacerova: drafting/revision of the manuscript for content, including medical writing for content; analysis or interpretation of data. M. Sealey: major role in the acquisition of data. L. Saldana: major role in the acquisition of data. W. Xiong: analysis or interpretation of data. M.R. Woodhall: major role in the acquisition of data. P.J. Waters: major role in the acquisition of data. T. Sénard: major role in the acquisition of data. J. Cheeseman: major role in the acquisition of data. P.A. Urbanowicz: major role in the acquisition of data. G.E. Hunt: major role in the acquisition of data. D.I.R. Spencer: drafting/revision of the manuscript for content, including medical writing for content; major role in the acquisition of data. James S.O. McCullagh: drafting/revision of the manuscript for content, including medical writing for content. M.I. Leite: major role in the acquisition of data. G.C. DeLuca: major role in the acquisition of data. J. Palace: major role in the acquisition of data. D.C. Anthony: drafting/revision of the manuscript for content, including medical writing for content; major role in the acquisition of data. T. Yeo: drafting/revision of the manuscript for content, including medical writing for content; major role in the acquisition of data; study concept or design; analysis or interpretation of data. F. Probert: drafting/revision of the manuscript for content, including medical writing for content; major role in the acquisition of data; study concept or design; analysis or interpretation of data.

Study Funding

T. Kacerova is funded by an EPSRC Doctoral Training Partnership (EP/W524311/1) and Numares AG (Am Biopark 9, 93053 Regensburg-Graß, Germany). T. Yeo is funded by the Singapore Ministry of Health's National Medical Research Council Clinician Scientist Award (CSAINV24jul-0004). F. Probert is funded by the Dorothy Hodgkin Early Career Fellowship in Chemistry in association with Somerville College.

Disclosure

T. Kacerova, M. Sealey, L. Saldana, W. Xiong, and M. Woodhall report no disclosures relevant to the manuscript. P. Waters is a named inventor on patents for antibody assays and has received royalties. He has received honoraria from Biogen Idec, Mereo Biopharma, Retrogenix, UBC, Euroimmun AG, UCB, F. Hoffmann La-Roche, and Alexion; travel grants from the Guthy-Jackson Charitable Foundation (GJCF); and research funding from Euroimmun AG and the GJCF. His work in the Autoimmune Neurology Diagnostic Laboratory is supported by the NHS Commissioning Service for NMOSD. T. Sénard was an employee of Ludger Ltd, United Kingdom. J. Cheeseman, P.A. Urbanowicz, G.E. Hunt, and D.I.R. Spencer are employees of Ludger Ltd, United Kingdom. J.S.O McCullagh, M.I. Leite, G. DeLuca, J. Palace, and D.C. Anthony report no disclosures relevant to the manuscript. T. Yeo has received honoraria from ASNA, AstraZeneca, Edanz Pharma, Euroimmun AG, Merck, Novartis, Roche, and Terumo BCT for consulting services and speaker's fees and research grants from the National Medical Research Council (NMRC Singapore), AstraZeneca, and Roche. He has also received travel grants and awards from PACTRIMS, ACTRIMS, ECTRIMS, Orebro University, UCB, and Merck. F. Probert reports no disclosures relevant to the manuscript.Go to Neurology.org/NN for full disclosures.

Publication History

Received by *Neurology® Neuroimmunology & Neuroinflammation* March 17, 2025. Accepted in final form August 21, 2025. Submitted and externally peer reviewed. The handling editor was Deputy Editor Anne-Katrin Pröbstel, MD.

References

1. Jurynczyk M, Probert F, Yeo T, et al. Metabolomics reveals distinct, antibody-independent, molecular signatures of MS, AQP4-antibody and MOG-antibody disease. *Acta neuropathologica Commun.* 2017;5(1):95. doi:10.1186/s40478-017-0495-8
2. Matthews L, Marasco R, Jenkinson M, et al. Distinction of seropositive NMO spectrum disorder and MS brain lesion distribution. *Neurology.* 2013;80(14):1330-1337. doi:10.1212/WNL.0b013e3182887957

3. Jurynczyk M, Geraldes R, Probert F, et al. Distinct brain imaging characteristics of autoantibody-mediated CNS conditions and multiple sclerosis. *Brain.* 2017;140(3):617-627. doi:10.1093/brain/aww350
4. Yeo T, Probert F, Jurynczyk M, et al. Classifying the antibody-negative NMO syndromes Clinical, imaging and metabolomic modeling. *Neurol Neuroimmunol Neuroinflamm.* 2019;6:e626. doi:10.1212/NXI.0000000000000626
5. Traub J, Häusser-Kinzel S, Weber MS. Differential effects of MS therapeutics on B cells-implications for their use and failure in AQP4-positive NMOSD patients. *Int J Mol Sci.* 2020;21(14):5021. doi:10.3390/ijms21145021
6. Palace J, Lin DY, Zeng D, et al. Outcome prediction models in AQP4-IgG positive neuromyelitis optica spectrum disorders. *Brain.* 2019;142(5):1310-1323. doi:doi:10.1093/brain/awz054
7. Selmaj K, Cree BAC, Barnett M, Thompson A, Hartung HP. Multiple sclerosis: time for early treatment with high-efficacy drugs. *J Neurol* 2024;271(1):105-115. doi:10.1007/s00415-023-11969-8
8. Yamamura T, Kleiter I, Fujihara K, et al. Trial of satralizumab in neuromyelitis optica spectrum disorder. *New Engl J Med.* 2019;381(22):2114-2124. doi:10.1056/NEJMoa1901747
9. Cree BAC, Bennett JL, Kim HJ, et al. Inebilizumab for the treatment of neuromyelitis optica spectrum disorder (N-MOmentum): a double-blind, randomised placebo-controlled phase 2/3 trial. *Lancet.* 2019;394(10206):1352-1363. doi:10.1016/S0140-6736(19)31817-3
10. Pittock SJ, Barnett M, Bennett JL, et al. Ravulizumab in aquaporin-4-positive neuromyelitis optica spectrum disorder. *Ann Neurol.* 2023;93(6):1053-1068. doi:10.1002/ana.26626
11. Meier S, Willemse EAJ, Schaedelin S, et al. Serum glial fibrillary acidic protein compared with neurofilament light chain as a biomarker for disease progression in multiple sclerosis. *JAMA Neurol.* 2023;80(3):287-297. doi:10.1001/jamaneurol.2022.5250
12. Probert F, Yeo T, Jurynczyk M, et al. Diagnosis and staging of multiple sclerosis using a metabolomics-based blood test: a simple method for monitoring progression independently of EDSS. *Mult Scler J.* 2019;25:500-501.
13. Yeo T, Sealey M, Zhou Y, et al. A blood-based metabolomics test to distinguish relapsing-remitting and secondary progressive multiple sclerosis: addressing practical considerations for clinical application. *Sci Rep.* 2020;10(1):12381. doi:10.1038/s41598-020-69119-3
14. Oppong AE, Coelewij L, Robertson G, et al. Blood metabolomic and transcriptomic signatures stratify patient subgroups in multiple sclerosis according to disease severity. *iScience.* 2024;27(3):109225. doi:10.1016/j.isci.2024.109225
15. Alwahsh M, Nimer RM, Dahabiyeh LA, et al. NMR-based metabolomics identification of potential serum biomarkers of disease progression in patients with multiple sclerosis. *Sci Rep.* 2024;14(1):14806. doi:10.1038/s41598-024-64490-x
16. Dickens AM, Larkin JR, Griffin JL, et al. A type 2 biomarker separates relapsing-remitting from secondary progressive multiple sclerosis. *Neurology.* 2014;83(17):1492-1499. doi:10.1212/WNL.0000000000000905
17. Wuhrer M, Selman MH, McDonnell LA, et al. Pro-inflammatory pattern of IgG1 Fc glycosylation in multiple sclerosis cerebrospinal fluid. *J Neuroinflammation.* 2015;12:235. doi:10.1186/s12974-015-0450-1
18. Yeo T, Probert F, Sealey M, et al. Objective biomarkers for clinical relapse in multiple sclerosis: a metabolomics approach. *Brain Commun.* 2021;3(4):fcab240. doi:10.1093/braincomms/fcab240
19. Mallagaray A, Rudolph L, Lindloge M, et al. Towards a precise NMR quantification of acute phase inflammation proteins from human serum. *Angew Chem Int Ed Engl.* 2023;62(35):e202306154. doi:10.1002/anie.202306154
20. Cvetko A, Kifer D, Gornik O, et al. Glycosylation alterations in multiple sclerosis show increased proinflammatory potential. *Biomedicines.* 2020;8(10):410. doi:10.3390/biomedicines8100410
21. Turčić A, Radovani B, Vogrinc Ž, et al. Higher MRI lesion load in multiple sclerosis is related to the N-glycosylation changes of cerebrospinal fluid immunoglobulin G. *Mult Scler Relat Disord.* 2023;79:104921. doi:10.1016/j.msard.2023.104921
22. Sy M, Newton BL, Pawling J, et al. N-acetylglucosamine inhibits inflammation and neurodegeneration markers in multiple sclerosis: a mechanistic trial. *J Neuroinflammation.* 2023;20(1):209. doi:10.1186/s12974-023-02893-9
23. Mortales CL, Lee SU, Manousadjian A, Hayama KL, Demetriou M. N-glycan branching decouples B cell innate and adaptive immunity to control inflammatory demyelination. *iScience.* 2020;23(8):101380. doi:10.1016/j.isci.2020.101380
24. Thompson AJ, Banwell BL, Barkhof F, et al. Diagnosis of multiple sclerosis: 2017 revisions of the McDonald criteria. *Lancet Neurol.* 2018;17(2):162-173. doi:10.1016/S1474-4422(17)30470-2
25. Wingerchuk DM, Banwell B, Bennett JL, et al. International consensus diagnostic criteria for neuromyelitis optica spectrum disorders. *Neurology.* 2015;85(2):177-189. doi:10.1212/WNL.0000000000001729
26. Banwell B, Bennett JL, Marignier R, et al. Diagnosis of myelin oligodendrocyte glycoprotein antibody-associated disease: international MOGAD Panel proposed criteria. *Lancet Neurol.* 2023;22(3):268-282. doi:10.1016/S1474-4422(22)00431-8
27. Jansen BC, Hafkenscheid L, Bondt A, et al. HappyTools: a software for high-throughput HPLC data processing and quantitation. *PLoS One.* 2018;13(7):e0200280. doi:10.1371/journal.pone.0200280
28. Jansen BC, Falck D, de Haan N, et al. LaCyTools: a targeted liquid chromatography-mass spectrometry data processing package for relative quantitation of glycopeptides. *J Proteome Res.* 2016;15(7):2198-2210. doi:10.1021/acs.jproteome.6b00171
29. Neelamegham S, Aoki-Kinoshita K, Bolton E, et al. Updates to the symbol nomenclature for glycans guidelines. *Glycobiology.* 2019;29(9):620-624. doi:10.1093/glycob/cwz045
30. Pucić M, Knezević A, Vidic J, et al. High throughput isolation and glycosylation analysis of IgG-variability and heritability of the IgG glycome in three isolated human populations. *Mol Cell Proteomics.* 2011;10:M111010090. doi:10.1074/mcp.M111.010090
31. Thévenot EA, Roux A, Xu Y, Ezan E, Junot C. Analysis of the human adult urinary metabolome variations with age, body mass index, and gender by implementing a comprehensive workflow for univariate and OPLS statistical analyses. *J Proteome Res.* 2015;14(8):3322-3335. doi:10.1021/acs.jproteome.5b00354
32. Duquette P, Pleines J, Girard M, Charest L, Senecal-Quevillon M, Masse C. The increased susceptibility of women to multiple sclerosis. *Can J Neurol Sci.* 1992;19(4):466-471. doi:10.1017/s0317167100041664
33. Papp V, Illes Z, Magyari M, et al. Nationwide prevalence and incidence study of neuromyelitis optica spectrum disorder in Denmark. *Neurology.* 2018;91(24):e2265-e2275. doi:10.1212/WNL.0000000000006645
34. Miclea A, Salmen A, Zoehner G, et al. Age-dependent variation of female preponderance across different phenotypes of multiple sclerosis: a retrospective cross-sectional study. *CNS Neurosci Ther.* 2019;25(4):527-531. doi:10.1111/cns.13083
35. Carnero Contentti E, Correale J. Neuromyelitis optica spectrum disorders: from pathophysiology to therapeutic strategies. *J Neuroinflammation.* 2021;18(1):208. doi:10.1186/s12974-021-02249-1
36. Filippi M, Rocca MA, Ciccarelli O, et al. MRI criteria for the diagnosis of multiple sclerosis: MAGNIMS consensus guidelines. *Lancet Neurol.* 2016;15(3):292-303. doi:10.1016/S1474-4422(15)00393-2
37. Inojosa H, Schriefer D, Ziemssen T. Clinical outcome measures in multiple sclerosis: a review. *Autoimmun Rev.* 2020;19(5):102512. doi:10.1016/j.autrev.2020.102512
38. Conroy LR, Hawkinson TR, Young LEA, Gentry MS, Sun RC. Emerging roles of N-linked glycosylation in brain physiology and disorders. *Trends Endocrinol Metab.* 2021;32(12):980-993. doi:10.1016/j.tem.2021.09.006
39. Pradeep P, Kang H, Lee B. Glycosylation and behavioral symptoms in neurological disorders. *Transl Psychiatry.* 2023;13(1):154. doi:10.1038/s41398-023-02446-x
40. Dojcsák D, Ilosvai AM, Vanyorek L, et al. N-functionalized magnetic nanoparticles for the N-glycomic analysis of patients with multiple sclerosis. *Int J Mol Sci.* 2022;23:9095.
41. Lakshmi Narasimhan R, Sharma G, Gopinath S. Exploring the molecular aspects of glycosylation in MOG antibody disease (MOGAD). *Curr Protein Pept Sci.* 2022;23(6):384-394. doi:10.2174/1389203723666220815110509
42. Radovani B, Gudelj I. N-glycosylation and inflammation; the not-so-sweet relation. *Front Immunol.* 2022;13:893565. doi:10.3389/fimmu.2022.893565
43. Kaneko Y, Nimmerjahn F, Ravetch JV. Anti-inflammatory activity of immunoglobulin G resulting from Fc sialylation. *Science.* 2006;313(5787):670-673. doi:10.1126/science.1129594
44. Sakae Y, Satoh T, Yagi H, et al. Conformational effects of N-glycan core fucosylation of immunoglobulin G Fc region on its interaction with Fcγ receptor IIIa. *Sci Rep.* 2017;7(1):13780. doi:10.1038/s41598-017-13845-8
45. Li J, Hsu HC, Ding Y, et al. Inhibition of fucosylation reshapes inflammatory macrophages and suppresses type II collagen-induced arthritis. *Arthritis Rheumatol.* 2014;66(9):2368-2379. doi:10.1002/art.38711
46. Gupta A, Gupta GS. Status of mannose-binding lectin (MBL) and complement system in COVID-19 patients and therapeutic applications of antiviral plant MBLs. *Mol Cell Biochem.* 2021;476(8):2917-2942. doi:10.1007/s11010-021-04107-3
47. Watkins LM, Neal JW, Loveless S, et al. Complement is activated in progressive multiple sclerosis cortical grey matter lesions. *J Neuroinflammation.* 2016;13(1):161. doi:10.1186/s12974-016-0611-x
48. Pröbstel AK, Zhou X, Baumann R, et al. Gut microbiota-specific IgA(+) B cells traffic to the CNS in active multiple sclerosis. *Sci Immunol.* 2020;5(53):eabc7191. doi:10.1126/sciimmunol.abc7191
49. Lassmann H. Pathogenic mechanisms associated with different clinical courses of multiple sclerosis. *Front Immunol.* 2018;9:3116. doi:10.3389/fimmu.2018.03116